Volume Title
ASP Conference Series, Vol. **Volume Number**
Author
© **Copyright Year** Astronomical Society of the Pacific

arXiv:1401.4761v1 [astro-ph.SR] 20 Jan 2014

Simulations of Accretion onto Magnetized Stars: Results of 3D MHD Simulations and 3D Radiative Transfer

Marina Romanova,[1] Ryuichi Kurosawa,[2]

Abstract.
We discuss the results of modelling of young magnetized stars, where matter flow is calculated using the three-dimensional (3D) magneto-hydrodynamic (MHD) *Cubed Sphere* code, and the spectra are calculated using the 3D Monte Carlo radiative transfer code *TORUS*. Two examples of modelling are shown: (1) accretion onto stars in stable and unstable regimes, and (2) accretion to a young star V2129 Oph, modelled with realistic parameters.

1. Introduction

The low-mass pre-main sequence solar-type stars evolve through different stages. Many of them are at the stage of a classical T Tauri star (CTTS), where the star becomes visible, but is still surrounded by a protoplanetary disk (e.g., Bouvier, et al. 2007). Observations show that CTTSs usually have a strong, dynamically important magnetic field. In these stars, the accretion disc is truncated by the magnetosphere, and the magnetic field governs the matter flow (e.g., Pringle & Rees 1972; Ghosh & Lamb 1979). The photometric and spectral variabilities of these stars are determined by the patterns of matter flow through the magnetosphere and by the shapes and positions of the hot spots. This problem is three-dimensional, so that the matter flow should be studied in global 3D MHD simulations, while photometry and spectra should be calculated using 3D radiative transfer approaches.

2. Numerical approaches

We perform global simulations of matter flow around magnetized young stars using the 3D MHD *Cubed Sphere* code, and afterwards use the obtained results for the calculation of spectra using the 3D radiative transfer code *TORUS*.

2.1. 3D MHD Simulations with *Cubed Sphere* code

We use the second-order Godunov-type three-dimensional (3D) MHD code developed by our group (Koldoba et al. 2002). It has many specific features which are oriented towards the efficient calculation of accretion onto a star with a tilted dipole or a more complex magnetic field: (1) the magnetic field $\mathbf{B}$ is decomposed into the "main" dipole component of the star, $\mathbf{B}_0$, and the component $\mathbf{B}_1$ induced by currents in the disc and the corona (Tanaka 1994); (2) the MHD equations are written in a reference frame rotating with the star; and (3) the numerical method uses the "cubed sphere" grid. The grid on the surface of the sphere consists of six sectors, with the grid in each sector being topologically equivalent to the grid on a face of a cube (e.g., Ronchi et al. 1996).

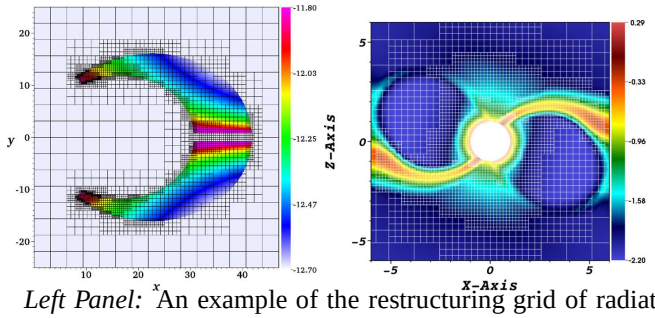

Figure 1. *Left Panel:* An example of the restructuring grid of radiative transfer code *TORUS* in the case where the funnel stream density and other parameters are determined by the analytical formula of Hartman et al. (1994) (from Kurosawa et al. 2004). *Right panel:* same as left panel, but for the case where the funnel flow was obtained in 3D MHD simulations (from Kurosawa et al. 2008).

We use a Godunov-type numerical scheme similar to the one described by Powell et al. (1999) and perform simulations in three dimensions. The full set of equations is the following:

$$\partial\rho/\partial t + \nabla\cdot(\rho\mathbf{v}) = 0,$$

$$\partial(\rho\mathbf{v})/\partial t + \nabla\cdot T = \rho\mathbf{g} + 2\rho\,\mathbf{v}\times\mathbf{\Omega} - \rho\,\mathbf{\Omega}\times(\mathbf{\Omega}\times\mathbf{R}),$$

$$\partial(\rho S)/\partial t + \nabla\cdot(\rho S\mathbf{v}) = 0\ ,$$

$$\partial\mathbf{B}/\partial t = \nabla\times(\mathbf{v}\times\mathbf{B}),$$

where $\mathbf{v}$ is the velocity of plasma in the rotating frame, $\mathbf{B}$ is the magnetic field, and S is the specific entropy. T is the stress tensor with components $T_{ik} \equiv p\delta_{ik} + \rho v_i v_k + (B^2\delta_{ik}/2 - B_iB_k)/4\pi$, and p is the gas pressure.

All variables are evaluated at the centers of the cells, and all vector variables are expressed in terms of their Cartesian components. Finite difference equations are then written for the variables. The finite difference scheme of Godunov's type has the form: $\mathcal{U}^{p+1} - \mathcal{U}^p/\Delta tV + \sum_{m=1..6} s_m\mathcal{F}_m = \mathcal{Q}$. Here, $\mathcal{U} = \{\rho,\ \rho\mathbf{v}, \mathbf{B},\ \rho S\}$ is the "vector" of the densities of conserved variables; $\mathcal{F}_m$ is the "vector" of flux densities normal to the face "m" of the grid cell, s_m is the area of the face "m", V is the volume of the cell, $\mathcal{Q}$ is the intensity of sources in the cell, and Δt is the time step. To calculate the flux densities $\mathcal{F}_m$, an approximate Riemann solver is used, analogous to the one described by Powell et al. (1999) (see also Kulikovski et al. 2001). The grid resolution is either $N_x = N_y = 51$ or 61 in each of the 6 blocks of the cube. The number of grid cells in the radial direction is $N_r = 150 - 180$.

2.2. 3D Radiative Transfer Code *TORUS*

For the calculations of hydrogen emission line profiles from the matter flow in the MHD simulations, we use the radiative transfer code *TORUS* (e.g. Harries 2000, 2011; Kurosawa et al. 2006, 2011; Kurosawa & Romanova 2012). In particular, the numerical method used in the current work is essentially identical to that in Kurosawa et al. (2011).

The basic steps for computing the line variability are as follows: (1) mapping the MHD simulation data onto the radiative transfer grid, (2) source function calculations, and (3) observed line profile calculations as a function of rotational phase.

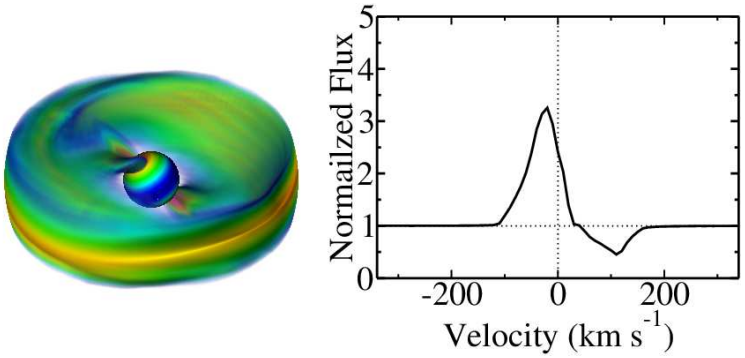

Figure 2. An example of accretion in the stable regime, where matter accretes in two ordered funnel streams (see density distribution in the left panel). The right panel shows the spectrum in Hδ hydrogen spectral line. The red-shifted absorption appears two times per period when the funnel stream crosses the line-of-sight. From Kurosawa & Romanova (2013).

In step (1), we use an adaptive mesh refinement (AMR) which allows for the accurate mapping of the original MHD simulation data onto the radiative transfer grid (Fig. 1). In step (2), we use a method similar to that of Klein & Castor (1978) (see also Rybicki & Hammer 1978; Hartmann, Hewett & Calvet 1994) in which the Sobolev approximation (e.g. Sobolev 1957; Castor 1970) is applied.

The Sobolev approximation works when the velocity gradient in the medium is large, such that a line center photon does not interact with the surrounding medium due to the Doppler effect, except for sharp resonance zones along a given direction. This essentially reduces the computation of the radiation field to a local problem, as opposed to a global problem. Normally, the radiation field at a given point in the medium depends on the radiation fields at all the points in the medium; hence, evaluating radiation fields in two or three dimensions is a computationally challenging problem. The use of the approximation significantly reduces the computational time, thus allowing us to make a multi-dimensional problem feasible. For example, the line profile averaged mean intensity at a given point can be expressed as (e.g., Rybicki & Hammer 1978)

$$\bar{J} = (1-\beta)\, S_l + I_{\rm c}\beta_{\rm c} \tag{1}$$

where S_l is the line source function and $I_{\rm c}$ is the intensity from the continuum radiation source (assuming no limb-darkening). The term S_l is local, i.e., it depends only on the conditions of local gas (e.g. level populations and so on), while $I_{\rm c}$ comes from a boundary condition. Further, the quantities β and $\beta_{\rm c}$ are the angle averaged escape probabilities of a photon from the point where $\bar{J}$ is evaluated, and they depend on the local quantities: the Sobolev optical depth $\tau_{\rm s}$ and the direction of photon propagation $\mathbf{n}$. The former can be expressed as

$$\tau_{\rm s} = \frac{c\chi_l}{\nu_l}\left|\frac{dv_{\mathbf{n}}}{dL}\right|^{-1}, \tag{2}$$

where c, χ_l and ν_l are the speed of light, line opacity, and line frequency, respectively. The last term $dv_{\mathbf{n}}/dL$ is the velocity gradient along the line element dL in the direction of the photon propagation $\mathbf{n}$.

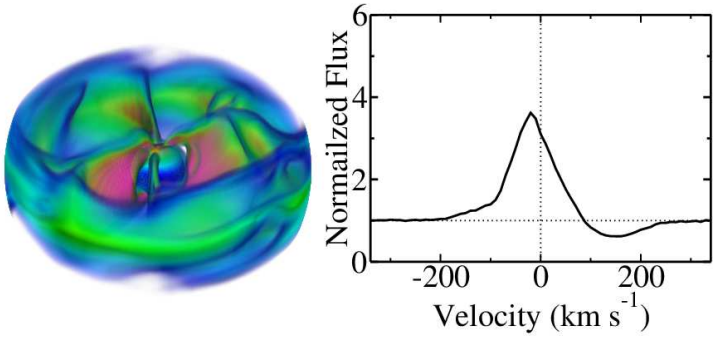

Figure 3. Same as in Fig. 2, but for the case of unstable accretion, where matter accretes in several unstable tongues and the red-shifted absorption varies irregularly, but is always present in the spectrum, because there are always tongues on the line-of-sight. From Kurosawa & Romanova (2013).

The populations of the bound states of hydrogen are assumed to be in statistical equilibrium, and the continuum sources are the sum of radiations from the stellar photosphere and the hot spots formed by the funnel accretion streams falling onto the stellar surface. Our model hydrogen atom consists of 20 bound and continuum states. For the photospheric contribution to the continuum flux, we adopt the effective temperature of the photosphere $T_{\rm ph} = 4000\,$K and the surface gravity $\log g_* = 3.5$ (cgs), and use the model atmosphere of Kurucz (1979). The sizes and shapes of the hot spots are determined by the local energy flux on the stellar surface (Romanova et al. 2004).

In step (3), the line profiles are computed using the source function computed in step (2). The observed flux at each frequency point in the line profiles is computed using the cylindrical coordinate system, with its symmetry axis pointing towards the observer. The viewing angles of the system (the central star and the surrounding gas) are adjusted according to the rotational phase of the star and the inclination angle of the system for each time-slice of the MHD simulations.

3. Examples of modelling

Here, we give two examples of modelling of young stars using 3D MHD + 3D radiative transfer approach.

3.1. Spectral diagnostics of stable and unstable regimes of accretion

A magnetized star with a dipole magnetic field may accrete in either stable or unstable regime (Romanova et al. 2008; Kulkarni & Romanova 2008). In the stable regime, matter flows above the magnetosphere in two ordered funnel streams, and the two hot spots on the surface of the star provide a nearly sinusoidal pattern of variability. In the unstable regime, matter penetrates between the magnetic field lines due to the magnetic Rayleigh-Taylor instability (e.g., Arons & Lea 1976). Simulations show that matter may accrete to the star in several unstable "tongues", which form irregular hot spots on the surface of the star, and the light-curve may be irregular. However, there are other possible causes for the irregular light-curves, such as frequent stellar magnetic flares, analogous to the solar flares, or accretion from a turbulent disk. Therefore, the irregular photometric light-curve alone is not a proof of unstable accretion. That is why we

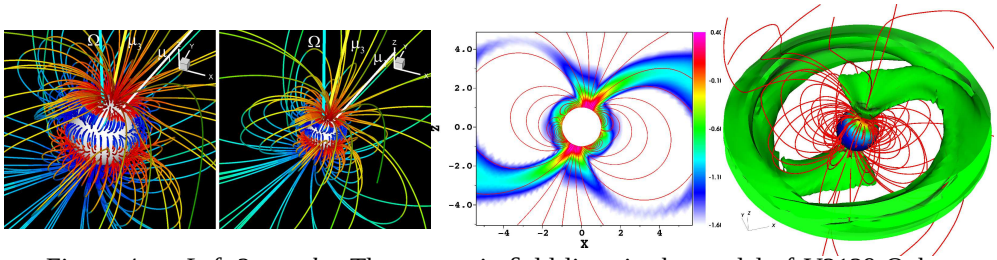

Figure 4. *Left 2 panels:* The magnetic field lines in the model of V2129 Oph, where the dipole and octupole components dominate. *Right two panels:* 2D and 3D views of matter flow around the modeled star V2129 Oph. From Romanova et al. (2011).

performed global 3D simulations of stable and unstable regimes of accretion, and used the results of simulations for the calculation of spectra in the Hydrogen spectral lines (Kurosawa & Romanova 2013). We chose 25 moments in time per rotational phase of the star, mapped the calculated values of matter flow (density, velocity, scaled temperature) to the AMR grid of the *TORUS* code and calculated the spectra for three rotations of the star (75 total). In the case of stable accretion, we observed that the spectrum has a typical red-shifted absorption when the funnel stream is on the line-of-sight between the star and the observer (see Fig. 2). It is absent when the funnel streams are away from the observer. In the unstable regime, matter flows to the star in several unstable tongues, and we observed red absorption all the time (see Fig. 3). In the unstable regime, the red-shifted absorption varies irregularly. This analysis may help to distinguish young stars accreting in the unstable regime. Many young, classical T Tauri stars (CTTSs) show irregular variability (Alencar, et al. 2010) on the time-scales corresponding to unstable accretion. Our analysis may help understand whether unstable accretion is responsible for this variability.

3.2. Modelling accretion onto V2129 Oph

Recently, the surface distribution of the magnetic field has been measured for several CTTSs. We chose one of these stars, V2129 Oph, and took the parameters of this star derived from observations: $M_* = 1.35M_\odot$, $R_* = 2.1R_\odot$, and period $P_* \approx 6.5$ days. The magnetic field of this star is dominated by the dipole component of $B_{dip} \approx 0.9$kG and octupole component of $B_{oct} \approx 2.1$kG, tilted at small angles about the rotational axis (Donati et al. 2011). We took the magnetic field configuration consisting of the dipole and octupole, and developed the MHD model based on these observed parameters of the star (see also Romanova et al. 2011). Fig. 4 shows the results of simulations. We mapped the results of simulations to the AMR grid of the *TORUS* code, and calculated the spectrum in different hydrogen lines. Fig. 5 shows that the observed spectrum is in good agreement with the modelled spectrum (Alencar, et al. 2012). This is an exciting example where a star with realistic parameters has been modelled in 3D MHD + 3D radiative transfer simulations, and the result has been compared with observations.

Acknowledgments. We thank the organizers for a very interesting meeting. Resources supporting this work were provided by the NASA High-End Computing (HEC) Program through the NASA Advanced Supercomputing (NAS) Division and the NASA Center for Computational Sciences (NCCS). The research was supported by NASA grant NNX11AF33G and NSF grant AST-1211318.

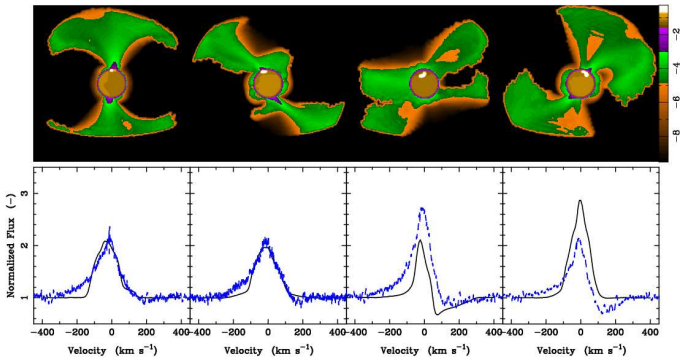

Figure 5. *Top panels:* Emissivity of the funnel flow calculated in the Hβ spectral line. *Bottom panels:* Comparison of the observed spectrum in Hβ line (blue line) with the modelled spectrum (black line). From Alencar et al. (2012).

References

Alencar, S.H.P., Teixeira, P.S., Guimaräes, M.M., McGinnis, P.T., Gameiro, J.F. et al. 2010, A&A, 519, A88

Alencar, S.H.P., Bouvier, J., Walter, F.M., Dougados, C., Donati, J.-F., Kurosawa, R., Romanova, M., et al. 2012, A&A, 541, 14

Arons J., Lea S. M., 1976, ApJ, 207, 914

Bouvier, J., Alencar, S.H.P., Harries, T.J., Johns-Krull, C.M., Romanova, M.M. 2007, in: B. Reipurth, D. Jewitt, and K. Keil (eds.), *Protostars and Planets V*, University of Arizona Press, Tucson, vol. 951, p. 479

Castor J. I., 1970, MNRAS, 149, 11

Donati, J.-F., Bouvier, J., Walter, F. M., et al. 2011, MNRAS, 412, 2454

Ghosh, P., Lamb, F.K. 1979, ApJ, 232, 259

Harries T. J., 2000, MNRAS, 315, 722

Harries T. J., 2011, MNRAS, 416, 1500

Hartmann L., Hewett R., Calvet N., 1994, 426, 669

Klein R. I., Castor J. I., 1978, ApJ, 220, 902

Koldoba A. V., Romanova M. M., Ustyugova G. V., Lovelace R. V. E. 2002, ApJ, 576, L53

Kulikovskii, A. G., Pogorelov, N. V., & Semenov, A. Y. 2001, Mathematical Aspects of Numerical Solution of Hyperbolic Systems (Boca Raton: Chapman & Hall)

Kulkarni, A., & Romanova, M.M. 2008, ApJ, 386, 673

Kurosawa R., Harries T. J., Bate M. R., Symington N. H., 2004, MNRAS, 351, 1134

Kurosawa R., Harries T. J., Symington N. H., 2006, MNRAS, 370, 580

Kurosawa R., Romanova M. M., Harries T. J., 2008, MNRAS, 385, 1931

Kurosawa R., Romanova M. M., Harries T. J., 2011, MNRAS, 416, 2623

Kurosawa R., Romanova M. M., 2012, MNRAS, 426, 2901

Kurosawa R., Romanova M. M., 2013, MNRAS, 431, 2673

Kurucz R. L., 1979, ApJS, 40, 1

Powell, K.G., Roe, P.L., Linde, T.J., Gombosi, T.I., & De Zeeuw, D.L. 1999, J. Comp. Phys., 154, 284

Pringle, J.E., Rees, M.J. 1972, A&A, 21, 1P

Romanova M. M., Ustyugova G. V., Koldoba A. V., Lovelace R. V. E.,. 2004, ApJ, 610, 920

Romanova M. M., Kulkarni A. K., Lovelace R. V. E., 2008, ApJ, 273, L171

Romanova, M. M., Long, M., Lamb, F. K., Kulkarni, A. K., Donati, J.-F. 2011, MNRAS, 411, 915

Ronchi, C., Iacono, R., & Paolucci, P.S. 1996, J. Comp. Phys. 124, 93

Rybicki G. B., Hummer D. G., 1978, ApJ, 219, 654

Sobolev V. V., 1957, Soviet Astronomy, 1, 678

Tanaka, T. 1994, J. Comp. Phys., 111, 381